SCALE-ADAPTIVE INVERSE IN 3D IMAGING

Dmitriy Paliy, Vladimir Katkovnik, Karen Egiazarian

Signal Processing Laboratory, Tampere University of Technology, P.O. Box 553, 33101 Tampere, Finland
e-mail: firstname.lastname@tut.fi

ABSTRACT

In this paper we propose a novel nonparametric approach to reconstruction of three-dimensional ($3D$) objects from $2D$ blurred and noisy observations. The proposed technique is based on an approximate image formation model which takes into account depth varying nature of the blur described by the point-spread function (PSF) of an optical system. The shift-invariantness of PSF in the depth is not required in the considered model. It is more general approach then typical $3D$ deconvolution problem with a shift-invariant PSF in all dimensions. The proposed restoration scheme incorporates regularized inverse and regularized Wiener inverse filters in combination with an adaptive denoising technique. The simulation results show efficiency of the developed approach.

1. INTRODUCTION

In a process of scene observation in a microscope or another optical device one can see well only the focused areas while others are observed as blurred. The problem arises as reconstruction of a $3D$ observed object from a set of $2D$ observations and it is classified to the family of deconvolution techniques.

Image deconvolution has become an established technique to improve both resolution and signal-to-noise ratio of serially sectioned three-dimensional images [1]. The reconstruction of $3D$ objects by means of optical sectioning is very popular in fluorescence microscopy imaging.

In general, images suffer from degradation due to the out-of-focused areas contributing to the in-focus areas. In a process of specimen observation in a microscope there is only one portion that appears in focus. However, usually a specimen is not flat but $3D$ structure. Therefore, some portions are out of focus. Nevertheless, these out-of-focus structures are in the field of view and thus obscure the in-focus plane. In order to obtain a deblurred $3D$ image of a specimen, it is common to use a method called *optical sectioning*. The microscope is focused at a given focal plane and the image is recorded. This image is an optical slice. Then, the microscope is refocused and another image is recorded. This process is repeated until the whole specimen is covered [2].

The $3D$ PSF is the main factor describing how a point source of light is being distributed laterally and across the focal planes. It plays a crucial role in image formation and its reconstruction. $3D$ deconvolution is a problem of object restoration from its observations using a known PSF of optical system. It is an ill-posed inverse problem [3]. It means that small perturbations in the initial data (observed image and inaccuracy in the used PSF model) result in large changes in the solution. For solving the deconvolution problem with a given PSF a number of approaches were proposed since the mid 1970s under various idealizations of the PSF and noise model.

In microscopy there are two approaches to reduce out-of-focus contributions: optical and computational. In the optical approach a confocal microscope is used that reduces the contribution from the out-of-focus fluorescence. The recorded clearer focal plane images are an optical equivalent of a series of microtome slices allowing a $3D$ reconstruction of a specimen.

In the computational approach, image processing is applied to process the set of $2D$ optical slices in order to reduce the out-of-focus interferences. This method is based on information about the processes of image formation. The most severe degradation is often caused by diffraction at objective and condenser lenses. This degradation is modeled by the PSF of the microscope optical system.

A number of techniques was proposed for optical sectioning based on the iterative expectation-maximization approach in [2],[4],[5]. Using the expectation-maximization formalism, algorithms for maximum-likelihood image restoration were developed using a depth-variant model for the optical sectioning microscopy. A modeling and estimation of PSF are considered. They also developed software for simulation of PSF. Theoretical analysis of properties for proposed techniques is an advantage. However, these methods are efficient but computationally expensive.

Also, the iterative solution presented by a combination of conjugate method with Tikhonov regularization is proposed in [1]. The conjugate gradient iteration scheme was used considering either Gaussian or Poisson noise models. For the regularization, the standard Tikhonov method was modified. However, the generic design of the algorithm allows for more regularization approaches. To determine the regularization parameter, the generalized cross-validation method was modified. Tests that were done on both simulated and experimental fluorescence wide-field data show reliable results.

There are a lot of works which exploit iterative inverse techniques, you can see also [6]. The noniterative Fourier-wavelet regularized deconvolution for $2D$ signals was described in [7]. The wavelet shrinkage is used to attenuate noise amplified during inversion operator. Authors also propose a method to determine regularization parameter providing near-optimal mean squared error results.

$3D$ sectioning microscopy equipped with digital deblurring algorithms is a powerful modern tool for visu-

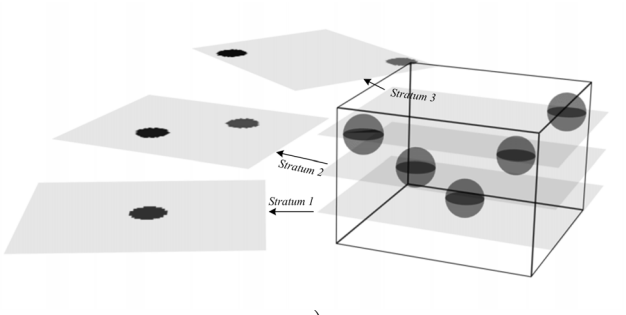

a)

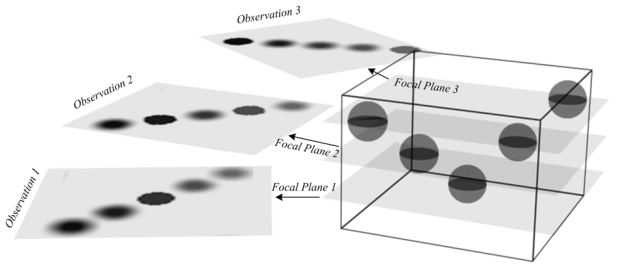

b)

Figure 1: $3D$ object consisted of 5 spheres: a) strata of the object; b) observation of each stratum focusing precisely at stratum 1, stratum 2, and stratum 3.

alization of specimens in biology, medicine, mineralogy, etc. Computational restoration methods applied to slice images are quite an efficient and prospective tool.

In this paper we focus on the noniterative approach. We generalize the spatially adaptive $2D$ deblurring algorithm developed in [8] to the $3D$ imaging. Nevertheless, the approach can also effectively incorporate iterative techniques, e.g. see [9].

We begin paper by providing a brief explanation of the problem in Section 2. Then, the proposed technique which incorporates inversion and denoising steps is given in Section 3. Finally, in Sections 4 and 5 we discuss implementation aspects and show results.

2. PROBLEM STATEMENT

Mathematically a variety of capturing principles can be described by the Fredholm integral of the first kind in $3D$ space $z(x) = \int v(x,t)y(t)dt$, where $x, t \in \mathbb{R}^3$, $v(t)$ is a $3D$ PSF of a system, $y(t)$ is a function of a real $3D$ object and $z(x)$ is an observed signal ([6],[10]). In general, PSF v is varying in all dimensions. A natural simplification is the assumption that it is shift-invariant which leads to a process formation by a convolution operation. When noise is involved, the approximate solution is

$$z(x) = (v \circledast y)(x) + \varepsilon(x), \tag{1}$$

where " $\circledast$ " denotes a $3D$ convolution operation and $\varepsilon(x)$ is a noise. In the continuous frequency domain the model (1) takes the form:

$$Z(\omega) = V(\omega) \cdot Y(\omega) + \varepsilon(\omega), \tag{2}$$

where $Z(\omega) = \mathcal{F}\{z(x)\}$, $\omega \in \mathbb{R}^3$, i.e. $\omega = (\omega_1, \omega_2, \omega_3)$, is a representation of a signal z in a Fourier domain and $\mathcal{F}\{\cdot\}$ is a Fourier Transform (FT), $V(\omega) = \mathcal{F}\{v(x)\}$, $Y(\omega) = \mathcal{F}\{y(x)\}$, $\varepsilon(\omega) = \mathcal{F}\{\varepsilon(x)\}$.

The assumption that the PSF is shift-invariant in all dimensions usually does not correspond to reality. A more natural assumption is that the PSF is invariant in (x_1, x_2) plane and varying in the third dimension x_3 [2], [4],[14]. This approach leads to the so-called optical sectioning formalism originated in digital microscopy and astronomy.

According to the technique the optical system is focused at some focal plane and an image is recorded, then it is focused at another plane and another image is recorded, and so on. The focusing planes may differ from the planes of interests. Precise focusing is not needed for the reconstruction. The only point is that the spatial resolution depends on a number of recorded images. This effect is illustrated in Section 5 by Fig.1,2.

Suppose that we wish to reconstruct a $3D$ image intensity function $y(x)$, $x \in \mathbb{R}^3$, from its blurred and noisy observation $z(x)$. In the argument $x = (x_1, x_2, x_3)$ the first two variables x_1 and x_2 define the pixel's coordinates of $2D$ image obtained from $y(x)$ with the fixed depth coordinate x_3. The axe x_3 is parallel to the optical axe of the microscope optical system and perpendicular to the 2D image plane.

We consider the discrete observation model in the following form:

$$z_i(\tilde{x}) = \sum_{j=1}^{m} (v_{i,j} \circledast y_j)(\tilde{x}) + \varepsilon_i(\tilde{x}), i = 1, ..., n, \tag{3}$$

where $\tilde{x} \in \mathbb{R}^2$ ($\tilde{x} = (x_1, x_2)$) are coordinates, i is a discrete variable used for the depth variable and $\mathbf{v} = (v_{i,j})$ is a matrix of the $2D$ $PSFs$. PSF $v_{i,j}$ corresponds to the observation of the object slice j from focusing at the position i. $\boldsymbol{\varepsilon} = (\varepsilon_1, ..., \varepsilon_n)$ is an additive noise which is assumed to be white Gaussian with zero mean and variance σ_i^2, $i = 1, ..., n$. It is required to restore the $3D$ image (object function $\mathbf{y}(\tilde{x}) = (y_1(\tilde{x}), ..., y_m(\tilde{x}))$) from n blurred $2D$ projections $\mathbf{z}(\tilde{x}) = (z_1(\tilde{x}), ..., z_n(\tilde{x}))$. Here, m is a number of physical slices of the object taken into consideration.

Consider the measured data consisting of a set of n images $z_i(\tilde{x})$, $i = 1, ..., n$, and $Z_i(\widetilde{\omega}) = \mathcal{F}\{z_i(\tilde{x})\}$ is their Fourier domain representation. Here $\widetilde{\omega} \in \{(\omega_1, \omega_2), \omega_i = 0, 1, ..., n_i - 1, i = 1, 2\}$ is the $2D$ normalized discrete frequency. Then, equation (3) in the frequency domain can be written as follows:

$$\begin{pmatrix} Z_1 \\ ... \\ Z_n \end{pmatrix} = \begin{pmatrix} V_{11} & ... & V_{1m} \\ ... & ... & ... \\ V_{n1} & ... & V_{nm} \end{pmatrix} \begin{pmatrix} Y_1 \\ ... \\ Y_m \end{pmatrix} + \begin{pmatrix} \varepsilon_1 \\ ... \\ \varepsilon_n \end{pmatrix}, \tag{4}$$

$V_{ij}(\widetilde{\omega}) = \mathcal{F}\{v_{ij}(\tilde{x})\}$, $Y_j(\widetilde{\omega}) = \mathcal{F}\{y_j(\tilde{x})\}$, and $\varepsilon_i(\widetilde{\omega}) = \mathcal{F}\{\varepsilon_i(\tilde{x})\}$. Finally, the collected $3D$ observation $\mathbf{Z} = (Z_1, ..., Z_n)^T$ is a set of blurred $2D$ images. In order to find the true object $\mathbf{Y} = (Y_1, ..., Y_m)^T$ we need to solve the system of linear equations (4).

The method feasibility depends on the properties of the matrix $\mathbf{V} = (V_{ij})$, $V_{ij} = \mathcal{F}\{v_{i,j}(\tilde{x})\}$, $i = 1, ..., n$, $j = 1, ..., m$.

We obtain for (4) the following vector-matrix equation defined in the $2D$ frequency domain:

$$\mathbf{Z}(\widetilde{\omega}) = \mathbf{V}(\widetilde{\omega})\mathbf{Y}(\widetilde{\omega}) + \boldsymbol{\varepsilon}(\widetilde{\omega}). \tag{5}$$

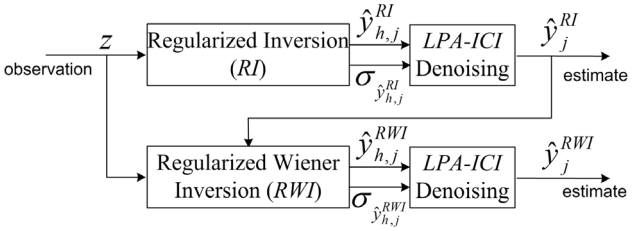

Figure 3: The proposed restoration scheme includes RI step with adaptive LPA-ICI denoising in order to obtain a reference signal for the RWI filter.

The equations (2) and (5) are similar but the difference is essential. The model (2) is assumed to be shift-invariant in all dimensions including x_3 particularly. On the contrary, the model (5) is shift-invariant in the plane $\widetilde{x} = (x_1, x_2)$ and can be shift-varying in x_3 dimension in general. As result, the product in Eq. (5) is not point-wise any more, but it is still point-wise in $\widetilde{\omega} \in \mathbb{R}^2$ domain.

An ill-posedness of restoration problem arises from small singular values of $\mathbf{V}(\widetilde{\omega})$ which after inversion would cause noise amplification. This is what makes the problem of restoration of $\mathbf{Y}(\widetilde{\omega})$ from $\mathbf{Z}(\widetilde{\omega})$ ill-posed. Different restoration techniques cope with it in a different way. In Section 3 we propose a novel approach to solve the problem.

Let us show an example to the problem. Fig.1 illustrates the idea. The $3D$ object consists of 5 spheres. The object slices lying in the planes perpendicular to the optical axe we will call *strata* [2]. It is assumed that the thickness of the strata is small and variation of the PSF with respect to the coordinate x_3 in one stratum is insignificant. The object in Fig.1 is discretized to $m = 3$ strata. In the object observations one can see clearly only the strata which are in the focal planes while others are seen blurred (Fig.1b). The aim is to reconstruct the original strata Fig.1a from their $n = 3$ observations Fig.1b.

3. PROPOSED TECHNIQUE

We develop the technique which is a vector-matrix generalization of the regularized inverse (RI) and regularized Wiener inverse (RWI) adaptive scale algorithms proposed in [8],[12]. The intersection of confidence intervals (ICI) rule [11] is exploited for the adaptive scale filtering of the reconstructed $2D$ slices of the $3D$ object function $\mathbf{y}(\tilde{x})$. The scheme consists of the two stages. At the first stage the RI filter and adaptive local polynomial approximation (LPA) with the ICI rule are used in order to obtain the estimate $\hat{\mathbf{y}}^{RI}(\tilde{x})$ exploited at the second stage as a reference signal. The second stage incorporates the RWI filter and LPA-ICI to obtain the final result $\hat{\mathbf{y}}^{RWI}(\tilde{x})$ (Fig. 3).

3.1 Regularized Inversion

The RI filter can be obtained as a least square solution of a penalized residual function for the problem (5) in the following form:

$$\mathbf{J} = \|\mathbf{Z}(\widetilde{\omega}) - \mathbf{V}(\widetilde{\omega})\mathbf{Y}(\widetilde{\omega})\|_2^2 + r_1^2 \|\mathbf{Y}(\widetilde{\omega})\|_2^2 =$$
$$= \sum_{\widetilde{w}} (\mathbf{Z}(\widetilde{\omega}) - \mathbf{V}(\widetilde{\omega})\mathbf{Y}(\widetilde{\omega}))^H (\mathbf{Z}(\widetilde{\omega}) - \mathbf{V}(\widetilde{\omega})\mathbf{Y}(\widetilde{\omega})) + \quad (6)$$
$$+ r_{RI}^2 \sum_{\widetilde{w}} \mathbf{Y}(\widetilde{\omega})^H \mathbf{Y}(\widetilde{\omega}),$$

where r_{RI}^2 is a regularization parameter and "^{H}" denotes the transpose complex-conjugate operation. The minimum of $\mathbf{J}^2$ is achieved when $\partial \mathbf{J}/\partial \mathbf{Y}^H = 0$. Calculation of this matrix derivative gives the equation for the estimate:

$$\widehat{\mathbf{Y}}^{RI}(\widetilde{\omega}) = (\mathbf{V}(\widetilde{\omega})^H \mathbf{V}(\widetilde{\omega}) + r_{RI}^2 \mathbf{I}_{m\times m})^{-1} \mathbf{V}^H(\widetilde{\omega}) \mathbf{Z}(\widetilde{\omega}), \quad (7)$$

where $\mathbf{I}_{m\times m}$ is the $m \times m$ identity matrix.

Following the technique proposed in [8],[12] we introduce the filtered RI estimate as follows:

$$\widehat{\mathbf{Y}}_h^{RI}(\widetilde{\omega}) = G_h(\widetilde{\omega}) \widehat{\mathbf{Y}}^{RI}(\widetilde{\omega}), \quad (8)$$

where G_h is the low-pass filter generated by LPA the same for all components of the vector $\widehat{\mathbf{Y}}^{RI}(\widetilde{\omega})$. Here, h is an important scale-parameter of a filter which is *selected adaptively* by the ICI rule. In spacial domain $\hat{y}_{h,j}^{RI}(\tilde{x}) = \mathcal{F}^{-1}\left\{\hat{Y}_{h,j}^{RI}(\widetilde{\omega})\right\}$, $j = 1, ..., m$. The idea and use of the LPA-ICI is described later.

Using formulas (5), (7), (8), and Parseval's theorem the variance at every point of the estimate $\hat{y}_{h,j}^{RI}(\tilde{x})$, $j = 1, ..., m$, is computed as

$$\sigma^2_{\hat{y}^{RI}_{h,j}(\tilde{x})} = var\{\hat{y}_{h,j}^{RI}(\tilde{x})\} =$$
$$= \frac{1}{n_1 n_2} \sum_{\widetilde{w}} (\mathbf{Q}_{RI}(\widetilde{\omega}) \boldsymbol{\sigma}^2 \mathbf{Q}_{RI}^H(\widetilde{\omega}))_{j,j}, \ j = 1, ..., m. \quad (9)$$

Here, $\mathbf{Q}_{RI}(\widetilde{\omega})$ is a transform matrix of (8) $\mathbf{Q}_{RI}(\widetilde{\omega}) = G_h(\widetilde{\omega})(\mathbf{V}(\widetilde{\omega})^H \mathbf{V}(\widetilde{\omega}) + r_{RI}^2 \mathbf{I}_{m\times m})^{-1} \mathbf{V}^H(\widetilde{\omega})$ and $\boldsymbol{\sigma}^2 = diag(\sigma_1^2, ..., \sigma_n^2)$ is a diagonal matrix of noise variances of observations $\mathbf{z}(\tilde{x}) = (z_1(\tilde{x}), ..., z_n(\tilde{x}))$. The variance of noise for every observation can be different in general. The variances of estimates $\left(\sigma^2_{\hat{y}^{RI}_{h,j}(\tilde{x})}\right)$ play a crucial role in the ICI rule for the adaptive data-driven scale h selection.

3.2 Regularized Wiener Inversion

Looking for an optimal linear estimate $\hat{y}_j(\tilde{x}) = (q_{j,i}^{WI} \circledast z_i)(\tilde{x})$, $i = 1, ..., n$, $j = 1, ..., m$, of a smoothed signal $y_{h,j}(\tilde{x}) = (g_h \circledast y_j)(\tilde{x})$ we come to the Wiener inverse filter $\mathbf{Q}_{WI} = \left(\mathcal{F}\{q_{j,i}^{WI}\}\right)$ by minimizing criterion function $\mathbf{J} = E\left\{\left\|\mathbf{Y}_h(\widetilde{\omega}) - \widehat{\mathbf{Y}}(\widetilde{\omega})\right\|_2^2\right\} = E\left\{\|G_h(\widetilde{\omega})\mathbf{Y}(\widetilde{\omega}) - \mathbf{Q}_{WI}(\widetilde{\omega})\mathbf{Z}(\widetilde{\omega})\|_2^2\right\}$. Solution of $\partial \mathbf{J}/\partial \mathbf{Q}_{WI}^H = 0$ gives us the transfer matrix for the Wiener filter:

$$\mathbf{Q}_{WI} = G_h \mathbf{Y}\mathbf{Y}^H \mathbf{V}^H (\mathbf{V}\mathbf{Y}\mathbf{Y}^H \mathbf{V}^H + n_1 n_2 \boldsymbol{\sigma}^2)^{-1}. \quad (10)$$

Inserting the regularization parameter r_{RWI}^2 into (10) we obtain the regularized Wiener inverse (RWI) filter:

$$\mathbf{Q}_{RWI} = \quad (11)$$
$$= G_h \mathbf{Y}\mathbf{Y}^H \mathbf{V}^H (\mathbf{V}\mathbf{Y}\mathbf{Y}^H \mathbf{V}^H + n_1 n_2 r_{RWI}^2 \boldsymbol{\sigma}^2)^{-1}.$$

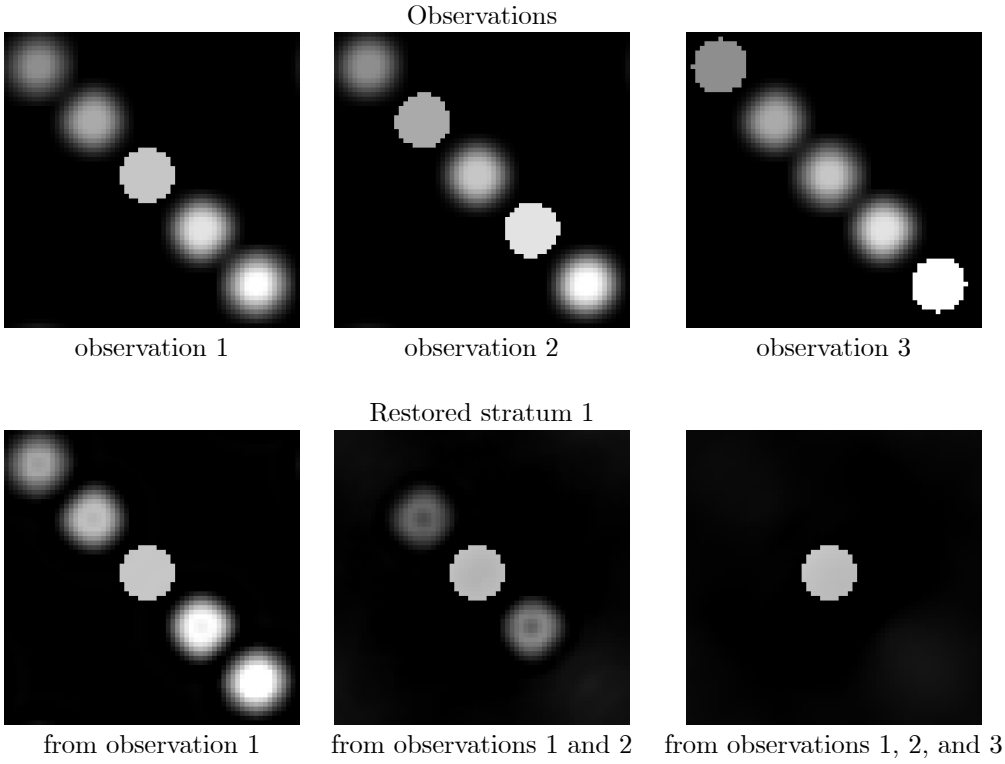

Figure 2: Example of reconstruction from noise-free observations of the object showed in Fig. 1. First row is the observations of stratum 1, 2, and 3 consiquently from left to right focusing precisely at each stratum. Second row is the examples of restoration of the stratum 1 from observation 1, observations 1 and 2, and from all 3 observations consiquently from left to right.

The regularization parameter r^2_{RWI} plays important role because of post-processing done by LPA-ICI, which produces a nonlinear estimate in general.

The filtered RWI estimate similarly to the (8) has the following form:

$$\widehat{\mathbf{Y}}_h^{RWI}(\widetilde{\omega}) = \mathbf{Q}_{RWI}(\widetilde{\omega})\mathbf{Z}(\widetilde{\omega}). \tag{12}$$

In spacial domain $\hat{y}^{RWI}_{h,j}(\tilde{x}) = \mathcal{F}^{-1}\left\{\hat{Y}^{RWI}_{h,j}(\widetilde{\omega})\right\}$, $j = 1, ..., m$. The variances for the estimate (12) are:

$$\sigma^2_{\hat{y}^{RWI}_{h,j}(\tilde{x})} = var\{\hat{y}^{RWI}_{h,j}(\tilde{x})\} = \tag{13}$$

$$= \frac{1}{n_1 n_2}\sum_{\widetilde{w}}(\mathbf{Q}_{RWI}(\widetilde{\omega})\boldsymbol{\sigma}^2\mathbf{Q}^H_{RWI}(\widetilde{\omega}))_{j,j},\ j = 1, ..., m,$$

and they are used in the following $LPA - ICI$ post-processing.

3.3 LPA-ICI Denoising

The LPA-ICI algorithm is a scale-adaptive denoising technique proposed in [8],[11],[12][13]. The LPA is a tool for linear filter design. In particular, the zero-order polynomial approximation is used in order to obtain the scanning window mean filters. The LPA also allows applying higher order polynomial approximations. Basically, in this paper, linear smoothing filter G_h in (8) and (12) is designed by means of LPA.

The ICI rule is the algorithm for the window size selection for every point $\widetilde{x}$. The idea of this approach is as follows. The algorithm searches for a largest local vicinity of the point of estimation where the LPA assumption fits well to the data. The estimates $\widehat{y}_{h,j}(\tilde{x})$, $j = 1, .., m$, are calculated for a grid of window sizes (scales) $h \in H = \{h_1, h_2, ..., h_J\}$, where $h_1 < h_2 < ... < h_J$. The adaptive scale is defined as the largest h^+ of those windows in the set H which estimate does not differ significantly from the estimators corresponding to the smaller window sizes. More detailed, a sequence of confidence intervals $D_k = \left[\widehat{y}_{h_k,j}(\tilde{x}) - \Gamma\sigma_{\hat{y}_{h_k,j}(\tilde{x})}, \widehat{y}_{h_k,j}(\tilde{x}) + \Gamma\sigma_{\hat{y}_{h_k,j}(\tilde{x})}\right]$, $k = 1, .., J$, is determined where $\Gamma > 0$ is a threshold parameter and $\sigma_{\hat{y}_{h_k,j}(\tilde{x})}$ is a standard deviation of estimate. The ICI rule can be stated as follows: *consider the intersection of confidence intervals* $I_k = \bigcap_{i=1}^{k} D_i$ *and let* k^+ *be the largest of the indeces* k *for which* I_k *is non-empty. Then the optimal scale* h^+ *is defined as* $h^+ = h_{k^+}$ *and, as result, the optimal scale estimate is* $\widehat{y}_{h^+,j}(\tilde{x})$. In the presented paper standard deviations $\sigma_{\hat{y}_{h_k,j}(\tilde{x})}$ of estimates are computed according to Eq. (9) and (13).

Theoretical analysis produced in [15] shows that this adaptive scale gives the best possible point-wise mean-squared error. *In practice this means that adaptively, for every sample, ICI allows the maximum degree of smoothing, stopping before oversmoothing begins* [16].

The threshold parameter Γ is a key parameter of the algorithm as it says when the difference between the estimates is large or small. Too large value of this parameter leads to signal oversmoothing and too small

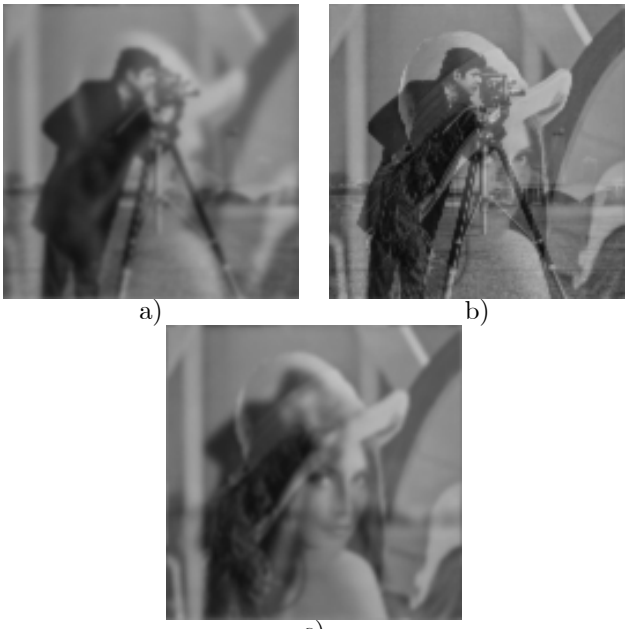

Figure 4: The noisy observations of Cameraman and Lena images obtained by focusing at different focal planes x_3=-1, x_3=0.5, and x_3=2.

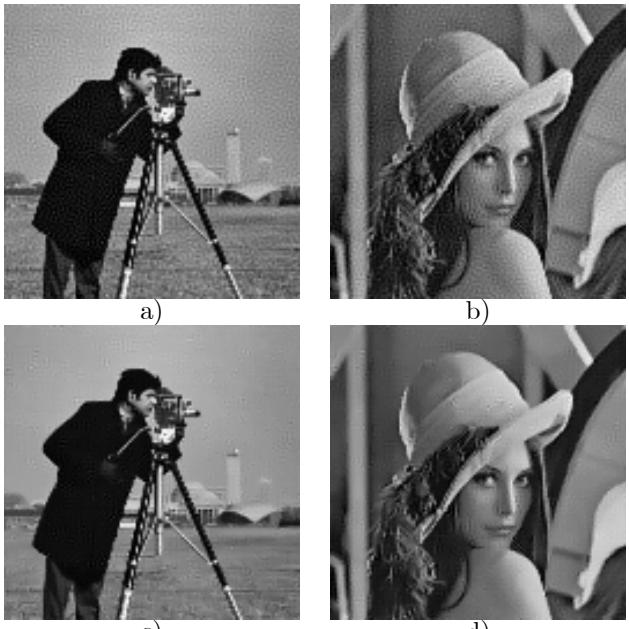

Figure 5: The reconstruction of Lena and Cameraman images from the mixed observations given in Figure 4: a) Regularized Inverse reconstructions of Cameraman, $RMSE$=0.0413; b) Regularized Inverse reconstructions of Lena, $RMSE$=0.0414; c) reconstructed Cameraman image by the Regularized Wiener filter with $LPA-ICI$ denoising, $RMSE$=0.0291; c) reconstructed Lena image by the Regularized Wiener filter with $LPA-ICI$ denoising, $RMSE$=0.0294.

value leads to undersmoothing. The reasonable value to preserve a signal and remove noise as mush as possible is somewhere between.

Optimal values of Γ can be derived from some heuristic and theoretical considerations (e.g. [8],[11],[12],[17]). In this paper we prefer to treat the threshold Γ as a fixed design parameter.

4. IMPLEMENTATION

4.1 PSF Simulation

The knowledge about a PSF and its properties is very important in a reconstruction technique. There are variety of commercial products to simulate or to measure a real PSF. We assume that the PSF is known and has Gaussian form: $v(x) = \frac{1}{\sqrt{2\pi}\sigma_{x_1}} \exp\left(-\frac{x_1^2}{2\sigma_{x_1}^2}\right) \cdot \frac{1}{\sqrt{2\pi}\sigma_{x_2}} \exp\left(-\frac{x_2^2}{2\sigma_{x_2}^2}\right) \cdot \frac{1}{\sqrt{2\pi}\sigma_{x_3}} \exp\left(-\frac{x_3^2}{2\sigma_{x_3}^2}\right)$. It is assumed that standard deviations of the Gaussian PSF in space perpendicular to optical axe are equal $\sigma_{x_1} = \sigma_{x2} = \sigma_{xy}$ and depend on x_3. In x_3 direction $v(x)$ has constant standard deviation $\sigma_{x_3} = \sigma_z$. So, $PSFs$ used in (3) are:

$$v_{i,j}(x_1, x_2) = \frac{1}{2\pi\sigma_{xy}^2(x_3(i) - x_3(j))} \exp\left(-\frac{x_1^2 + x_2^2}{2\sigma_{xy}^2(x_3(i) - x_3(j))}\right) \cdot \frac{1}{\sqrt{2\pi}\sigma_z} \exp\left(-\frac{(x_3(i) - x_3(j))^2}{2\sigma_z^2}\right), \quad (14)$$

where $i = 1, ..., n$, $j = 1, ..., m$.

The value of σ_z is very important because it is directly related to conditional number of the matrix $(v_{i,j})$, i.e. with an ability to solve the system of equations (4). Physically it means how strong a contribution of jth stratum to the observation at ith focal plane. When $\sigma_z \to 0$ the observation $z_i(\widetilde{x})$ consists only of the stratum at a focus $y_j(\widetilde{x})$ $(i = j)$ and there is no need to make a reconstruction. On the other hand, $\sigma_z \to \infty$ and the observation consists of all possible strata which blurred and equally visible. In this case, reconstruction is *impossible* even in theoretically ideal noise-free conditions. In all experiments σ_z is fixed to value 4.

In simulations σ_{xy} depends on the distance between focal plane i and stratum j :

$$\sigma_{xy} = k\,|x_3(i) - x_3(j)|\,, \quad (15)$$

where k is some coefficient of proportionality. The meaning of σ_{xy} is the jth stratum as blurred as it is far from plane of focusing.

The PSF is normalized in such a way that $\sum_{j=1}^{m} \sum_{\widetilde{x}} v_{i,j}(\widetilde{x}) = 1$.

However, in practice σ_z and σ_{xy} are usually variable because of imperfection of optics and other physical phenomena. In this paper, theoretically we demand only invariance of $\sigma_{xy}(x_1, x_2) = const$.

4.2 Noise Level

We used a modified blurred signal-to-noise ratio ($BSNR$) for evaluation of the level of the noise in our

	Cameraman	Lena
RI	0.0413	0.0414
RI with $LPA-ICI$	0.0318	0.0313
RWI	0.0323	0.0316
RWI with $LPA-ICI$	0.0291	0.0294

Table 1: $RMSE$ values obtained by the proposed algorithms.

	Cameraman	Lena
RI	27.68	27.66
RI with $LPA-ICI$	29.94	30.08
RWI	29.81	29.99
RWI with $LPA-ICI$	30.73	30.61

Table 2: $PSNR$ (dB) values obtained for the proposed algorithms.

experiments:

$$BSNR_i = 10\log_{10}\left(\frac{\left\|\sum_j (v_{i,j} \circledast y_j)(\tilde{x}) - \frac{1}{\#}\sum_{\tilde{x}}\Big(\sum_j (v_{i,j} \circledast y_j)(\tilde{x})\Big)\right\|_2^2}{n_1 n_2 \sigma_i^2}\right),$$

where $i = 1, ..., n$ and $j = 1, ..., m$.

In estimation and filtering we assume that the level of the noise is unknown and estimated (see algorithms in [18],[19]).

5. EXPERIMENTS

In this section we present simulation results illustrating a performance of the developed technique.

One of the used models is shown in Fig.1. A $3D$ object consists of 5 nonoverlapping spheres. A simplified discrete model of this object is given by 3 strata shown in Fig.1a. Observations are produced by focusing the optical system on each stratum Fig.1b. These three $2D$ observation-images are used for reconstruction of the images in the three strata. The reconstruction results are given in Fig.2. It is assumed that the observations are noiseless and the pure inverse procedure is used. It means that in the RI algorithm $r_{RI} = 0$.

The left image in the second row of Fig.2 shows reconstruction of the stratum 1 from the observations obtained from a single observation-image corresponding to focusing precisely at the stratum 1 (focal plane 1). Naturally, this reconstruction is identical to the observation-image shown in the first row of this figure (left). Thus, the stratum 1 is in focus while the strata 2 and 3 are blurred.

The middle image of the second row shows the reconstruction of the same stratum 1 done from the observations of two strata 1 and 2. It is seen that the interference of planes 2 and 3 is lower in this reconstruction. The right image of the second row demonstrates the perfect reconstruction of the stratum 1. This result is obtained using for reconstruction all three observation-images 1, 2 and 3. The experiment confirms that the algorithm is able to give perfect reconstruction when sufficient number of observations is available and there is no noise.

A second group of experiments concerns noisy data and is used to demonstrate how a redundancy of observations allows to filter data and reduce a strong interference of different images. Let the object be a composition of 2 parallel strata. The test-images Cameraman and Lena (downsampled to the size 128×128) are used as images in these strata.

The coordinates of the image-strata are $x_3 = 0$ and $x_3 = 1$ for the Cameraman and Lena images, respectively. The observations are produced by focusing at the focal planes with the coordinates $x_3 = -1$, $x_3 = 0.5$, and $x_3 = 2$. The obtained observations with a strong interference of the images are seen in Fig.4. The parameter k in the formula (15) is equal to 1. It defines a level of the blur of the observations obtained in different focal planes. For instance, for the observations at focal plane $x_3 = -1$, the Cameraman image is seen blurred with $\sigma_{xy} = 1$ and the Lena image is seen blurred stronger with $\sigma_{xy} = 2$. The corresponding observations are shown in Fig.4a. In Fig.4c the Cameraman image is more blurred then the Lena image and the both images are equally blurred in Fig.4b.

We set the additive noise variances σ_i^2, $i = 1, 2, 3$, in such a way that $BSNR \simeq 40$ dB. It gives the values $\sigma_1 = 0.0014$, $\sigma_2 = 0.0016$, $\sigma_3 = 0.0014$. These standard deviations are small. Nevertheless, noise effects are well-visible in the reconstructed images (Fig.4,5).

The criteria used to evaluate the algorithm performance are the square root mean squares error ($RMSE$)

$$RMSE_i = \sqrt{\frac{1}{n_1 n_2}\sum_{\tilde{x}} \left(y_i(\tilde{x}) - \hat{y}_i(\tilde{x})\right)^2},$$

and peak signal-to-noise ratio ($PSNR$)

$$PSNR_i = 10\log_{10}\left(\frac{\max_{\tilde{x}}(y_i(\tilde{x}))^2}{\frac{1}{n_1 n_2}\sum_{\tilde{x}}\left(y_i(\tilde{x}) - \hat{y}_i(\tilde{x})\right)^2}\right),$$

where i numbers the reconstructed images in the strata 1 and 2, $i = 1$ for Cameraman and $i = 2$ for Lena.

The directional LPA is applied for the filters in (8) and (12). We use the first-order polynomial approximation along the main radial direction of the sectorial window and the zero-order approximation for the perpendicular direction [11],[12],[13]. We used 8 sectorial directional kernels with the window lengths defined by the set $H_1 = \{1, 5, 9, 15, 33\}$ and the window width defined by the set $H_2 = \{1, 1, 1, 2, 2\}$. The ICI threshold parameters are fixed at $\Gamma = 2$ and $\Gamma = 4$ for RI and RWI algorithms, respectively.

The results for $RMSE$ and $PSNR$ are shown in Tables 1, 2. The rows RI and RWI are given for the algorithms without $LPA-ICI$ filtering. The rows RI with $LPA-ICI$ and RWI with $LPA-ICI$ are given for the algorithms where $LPA-ICI$ filtering is used.

Regularization parameters for the RI and RWI algorithms are fixed as follows $r_{RI} = 0.0075$ and $r_{RWI} = 0.039$.

In order to obtain good results for the $LPA-ICI$ denoising the regularization parameters should take

smaller values. In our experiments we use the values of the regularized parameter shown above divided by 2.

The figures in the tables show a successive performance improvement caused by the $LPA-ICI$ filtering as well as using the RWI instead of the more simple RI algorithm. The RWI algorithm always gives the best result.

Fig.5a,b demonstrate the reconstructed images obtained after the RI algorithm. It is seen that these images are quite noisy. The images obtained by the RWI with $LPA-ICI$ algorithm are shown in Fig.5c,d. They are well-denoised and the edges are well-preserved. However, some minor artifacts can be noticed.

A *MATLAB* implementation of the developed algorithms is available at *http://www.cs.tut.fi/~lasip/*.

6. CONCLUSIONS

Computational sectioning imaging is known to be efficiency for three dimensional inverse imaging. However, the ill-conditioning of the PSF results in a high sensitivity of the inverse with respect to even small noises and disturbance. In this paper we propose a new technique with a good potential for high-resolution $3D$ image reconstruction and efficient noise suppression. The technique is a generalization of the algorithms for $2D$ inverse imaging developed in [8]. Efficient deconvolution algorithms in combination with a point-wise adaptive denoising make this approach powerful tool for the visualization of $3D$ objects in microscopy, astronomy, or in everyday digital photo-images.

REFERENCES

[1] Schaefer L. H., Schuster D., Herz. H., "Generalized Approach for Accelerating Maximum Likelihood Based Image Restoration Applied to Three-Dimensional Fluorescence Microscopy", *Journal of Microscopy*, Vol. 204, Pt.2, pp. 99-107, Nov. 2001.

[2] Preza C., Conchello J., "Depth-Variant Maximum Likelihood Restoration for Three-Dimensional Fluorescence Microscopy", *Journal of Optical Society of America A*, No. 9, Vol. 21, Sep. 2004.

[3] Tikhonov A. N., Arsenin V. Y., *Solutions of Ill Posed Problems,* Willey, New York, 1977.

[4] Markham J., Conchello J., "Fast Maximum-Likelihood Image Restoration Algorithms for Three-Dimensional Fluorescense Microscopy", *Journal of Optical Society of America A*, 18, pp. 1062-1071, 2001.

[5] McNally J., Karpova T., Cooper J., and Conchello J., "Three-dimensional imaging by deconvolution microscopy, " Methods, vol.19, pp. 373-385, 1999.

[6] Zhu D., Razaz M., Lee R., "A Landweber Algorithm for 3D Confocal Microscopy Restoration", Proceedings of the 17th International Conference on Pattern Recognition, ICPR 2004, Vol. 1, Pp. 552 - 555, Aug. 2004.

[7] Neelamani R., Choi H., and Baraniuk R. G., "Forward: Fourier-wavelet regularized deconvolution for ill-conditioned systems". *IEEE Trans. on Image Proc., 2003.*

[8] Katkovnik V., Egiazarian K. and Astola J., "A spatially adaptive nonparametric image deblurring," IEEE Transactions on Image Processing, In print.

[9] Trimeche M., Paliy D., Vehvilainen M., Katkovnik V., "Multi-Channel Image Deblurring of Raw Color Components", Proceedings of SPIE, Volume 5674, Computational Imaging III, pp. 169-178, March 2005.

[10] Rushforth C., *Image Recovery: Theory and Application, Chap. Signal Restoration, functional analysis, and Fredholm integral eguations of the first kind.* Academis Press, 1987.

[11] Katkovnik V., "A new method for varying adaptive bandwidth selection", *IEEE Trans. on Signal Proc.,* vol. 47, no. 9, pp. 2567-2571, 1999.

[12] Katkovnik V., K. Egiazarian, and J. Astola, *Adaptive varying scale methods in image processing,* Tampere International Center for Signal Processing, TICSP Series, no. 19, Tampere, TTY, Monistamo, 2003.

[13] Katkovnik, V., A. Foi, K. Egiazarian, and J. Astola, "Directional varying scale approximations for anisotropic signal processing", Proc. XII European Signal Proc. Conf., EUSIPCO 2004, Vienna, pp. 101-104, September 2004.

[14] Ng M. K., "Total Variation Based Image Restoration of Three Dimensional Microscopic Objects", *TENCON '96. Proceedings, 1996 IEEE TENCON, Digital Signal Processing Applications*, Vol. 1, 26-29, pp. 288-293, Nov. 1996

[15] Goldenshluger A., and Nemirovski A., "On spatial adaptive estimation of nonparametric regression", *Math. Meth. Statistics*, vol. 6, pp. 135 – 170, 1997.

[16] Foi A., Katkovnik V., Egiazarian K., and Astola J., "Inverse halftoning based on the anisotropic LPA-ICI deconvolution", In: Astola, J. et al. (eds). Proceedings of The 2004 International TICSP Workshop on Spectral Methods and Multirate Signal Processing, SMMSP 2004, Vienna, Austria, 11-12 September 2004, pp. 49 – 56, 2004.

[17] Stanković L., "Performance analysis of the adaptive algorithm for bias-to-variance tradeoff", *IEEE Trans. on Signal Proc.*, vol. 52, No. 5, pp. 1228 – 1234, 2004.

[18] Hampel F.R., Ronchetti E.M., Rousseeuw P.J., and Stahel W.A., *Robust Statistics, The Approach Based on Influence Functions.* Wiley: New York, 1986.

[19] Donoho D.L., "De-noising by soft-thresholding", *IEEE Trans. Inform. Theory*, vol. 41, pp. 613-627, May 1995.